applied sciences

MDPI

Article

Integrated Carbonate Rock Type Prediction Using Self-Organizing Maps in E11 Field, Central Luconia Province, Malaysia

Grisel Jiménez Soto [1,*], Abdul Halim Abdul Latiff [1], Wael Ben Habel [2], Saw Bing Bing [3] and Michael Poppelreiter [4]

[1] Centre for Subsurface Imaging, Institute of Hydrocarbon Recovery, Universiti Teknologi PETRONAS, Seri Iskandar 32610, Malaysia; abdulhalim.alatiff@utp.edu.my
[2] Schlumberger Wta Malaysia Sdn Bhd, Ground Floor, Wisma Rohas Pure Circle, No. 9, Jalan P Ramlee, Kuala Lumpur 50250, Malaysia; whabel@slb.com
[3] The South-East Asia Carbonate Research Laboratory, Universiti Teknologi PETRONAS, Seri Iskandar 32610, Malaysia; bingbing.saw@utp.edu.my
[4] Shell Kuwait Exploration and Production BV, P.O. Box 28487, Safat 13145, Kuwait; m.poppelreiter@shell.com
* Correspondence: jimenezsotogrisel@gmail.com

Abstract: Reducing uncertainty in 3D carbonate rock type distribution is a critical factor that profoundly impacts field development for hydrocarbon or carbon capture and storage (CCS) projects. Miocene carbonate reservoirs in the Central Luconia offshore region are economically important global gas reservoirs. The nature of these carbonate rocks can be visually distinct in the core and the multiscale reservoir heterogeneity might vary in scale from the 100-m scale to the sub-millimeter scale. This work presents a series of steps workflow to obtain spatial information about the organization scheme of carbonate rock types, and capture the most important petrophysical and sedimentary controls on rock property distribution in the E11 field, a carbonate buildup, located in Central Luconia Province, offshore Malaysia. The spatial data were generated from a supervised neural Kohonen algorithm. The rock types predicted with this workflow were propagated using IPSOM probabilized self-organizing maps SOM. This tool is used for classifying multivariate data samples according to "patterns" or multivariate responses. The workflow includes several steps: A Step 1—Core data description, B Step 2—Thin section description, C Step 3—Well log interpretation, and D Step 4—IPSOM probabilized self-organizing maps for facies prediction SOM. The depth plots of the predicted rock type showed close correspondence to the core-based rock types in terms of the stratigraphic organization of tight and reservoir layers, proportions, and juxtaposition. This result is sufficient to merit the application of the rock type logs into a future porosity model of the E11 field, and to understand the lateral and vertical distribution of tight and reservoir rock types of distribution. The results can be used to build a future realistic digital twin of the subsurface, and in digital geological modeling.

Keywords: carbonate rock type; Kohonen self-organizing maps; Central Luconia

check for updates

Citation: Jiménez Soto, G.; Abdul Latiff, A.H.; Ben Habel, W.; Bing Bing, S.; Poppelreiter, M. Integrated Carbonate Rock Type Prediction Using Self-Organizing Maps in E11 Field, Central Luconia Province, Malaysia. *Appl. Sci.* **2022**, *12*, 7688. https://doi.org/10.3390/app12157688

Academic Editor: Fabrizio Balsamo

Received: 18 May 2022
Accepted: 20 June 2022
Published: 30 July 2022

Publisher's Note: MDPI stays neutral with regard to jurisdictional claims in published maps and institutional affiliations.

Copyright: © 2022 by the authors. Licensee MDPI, Basel, Switzerland. This article is an open access article distributed under the terms and conditions of the Creative Commons Attribution (CC BY) license (https://creativecommons.org/licenses/by/4.0/).

1. Introduction

Shallow-water carbonate reef complexes occurred in Southeast Asia during the Tertiary [1,2]. Buried in the subsurface, these carbonate coral atolls of the Miocene age are important hydrocarbon reservoirs in SE Asia and globally.

The E11 field is located in the Central Luconia province of the South China Sea. The field is located 300 Km from the present coastline, offshore Sarawak, Borneo (Figure 1). Several past studies [3–10] revealed several reservoir heterogeneities that can be observed, including (a) horizontal and (b) vertical, related to carbonate deposition, such as reef and slope facies, and associated faulting that often fringes carbonate platforms [9].

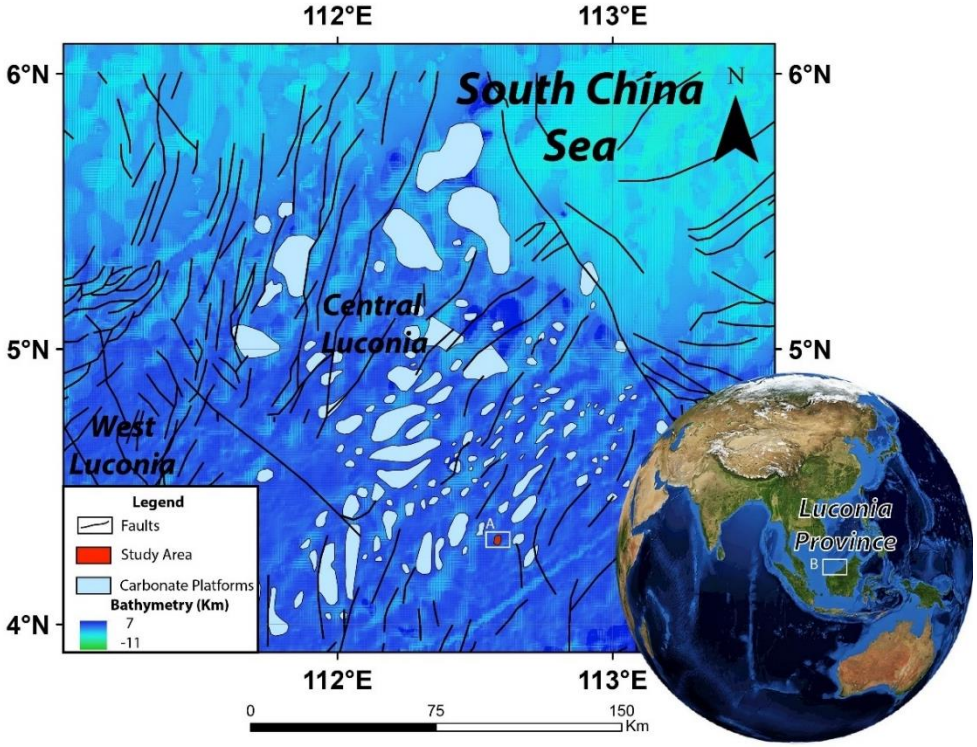


Figure 1. The location and bathymetry map of Central Luconia province and surroundings (**A**) in the white square, where the geology province is located, and in the red square, where the E11 field is located; (**B**) Central Luconia province geographic location.

The distribution of reservoir properties within these carbonate buildups (pore types, porosity, grain density, permeability) is probably an expression of the global or regional environmental factors, leading to exposure and flooding-related reservoir quality changes [11]. Thus, this highlights the need for a solid understanding of the original rock fabrics/facies, associated depositional environments, diagenetic modifications, and their petrophysical expression to consolidate lithofacies, petrophysical groups, and rock types that can be distributed in a geologically realistic manner during reservoir modeling. This distinction controls both the static and dynamic characteristics of a reservoir while linking geological attributes to spatial trends [12].

Primary depositional facies variability and stacking architecture, diagenetic overprint, and faults and fractures are the common controls on reservoir compartmentalization and high-permeability pathways and thus flow behavior in hydrocarbon reservoirs [13]. According to [14], rock properties are most commonly co-vary with porosity. Hence, there is a need for genetic rock typing in carbonates to improve the prediction of permeability and saturation behavior.

In this work, rock types derived from core data are discussed in detail from one of these hydrocarbon-bearing buildups, the E11 field. The core data from two wells, wireline logs of 10 wells, and top markers are correlated in terms of flooding intervals, defining three main carbonate reservoir zones, divided by four tight layers corresponding to major flooding events.

The E11 data are used to illustrate a workflow that makes use of a proxy of well log data for rock typing propagation in wells where the core is not available. The E11 field was chosen as a case study because the field was extensively studied in the past [1,4–10,15].

IPSOM probabilized self-organizing maps of the rock typing seek to optimize geological and petrophysical characterization from the core and log data. A core-based rock type scheme is defined based on the recognition of lithology, depositional facies, dominant pore types, porosity, and permeability characteristics. As a pre-requisite, sedimentological evaluation of cores provides the depositional and diagenetic frameworks and controls on

pore types and geometries [16]. The rock types of distribution within the well are discussed, with the identification of relationships between the rock types and the stratigraphy.

2. Study Area

The Central Luconia province covers an area of some 45,000 Km^2 [17] and is endowed with over 250 buildups and some platform sizes of more than 200 Km^2, one of the largest carbonate provinces in Southeast Asia [11]. The platform architecture of carbonate buildups in Central Luconia is indicated by numerous similarities and differences (Figure 1). The facies composition on the northern and southern buildups shows similar components on all buildups, with major components consisting of foraminifera, red algae, and a variety of corals [18].

The E11 field has already been the subject of several geological and seismic studies, including [3,4,9,10,15]. The E11 field is located in the Central Luconia province in the South China Sea, 100–300 km from the present coastline, offshore Sarawak, Borneo, in water depths of 60–140 m. The E11 structure is a pinnacle buildup of 7 by 9 Km in size, laterally interfingering with Cycle V clastics in its upper part. The depth of the top buildup is approximately 1500 m. The thickness of the buildup is 650 m, with an overall areal extent of 7.3 × 10.3 Km (Figure 2). The age of the carbonate buildup is interpreted as the Middle to Late Miocene age based on biostratigraphic studies [3] and 16 Ma to 12.3 Ma based on Sr dating [11].

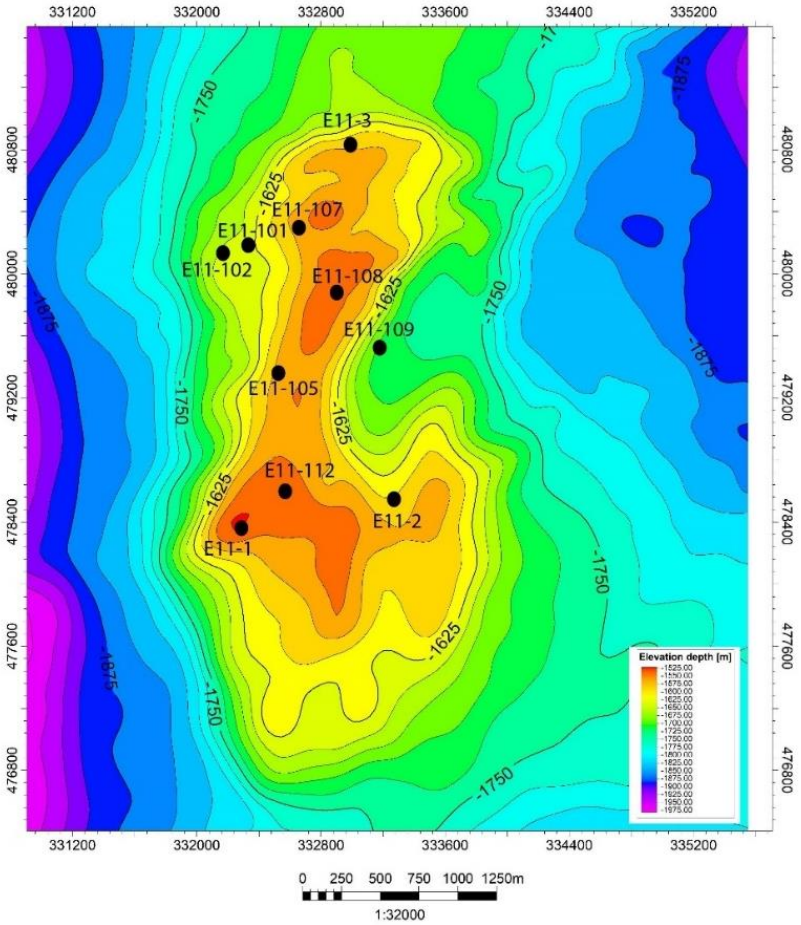


Figure 2. Base map of the carbonate map structure with the location of the 10 wells used for this study.

Geomorphologically, the field consists of a lower megaplatform complex and an upper pinnacle stage (Figure 3).

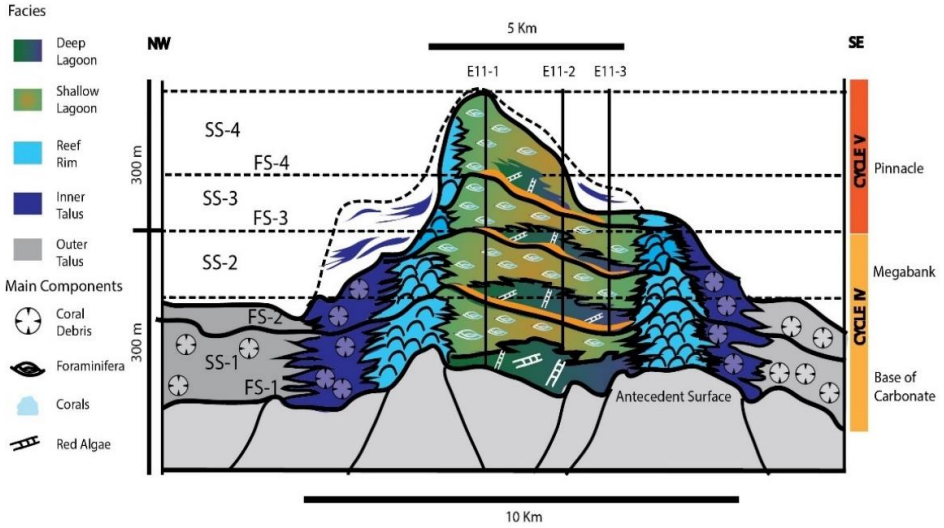


Figure 3. Characteristics and sequence stratigraphic conceptual model of E11 field.

- **Megaplatform complex Cycle IV FS1, SS1, FS2, and SS2**

The widespread megabank sequence began with the deposition of the basal transgressive unit BTU of the Cycle IV carbonates [3,11,17]. In this study, this interval corresponds to 2 reservoir zones, SS1 and SS2, divided by three tight intervals FS1, FS2, and FS3. FS3 corresponds to a transgression level ending with shallow megabank carbonate sedimentation corresponding to "a transgressive event" [8].

- **Pinnacle carbonate Cycle V F3S, SS3, FS4, SS4**

This stage corresponds to a steep flanked and smaller buildup above the FS3 interval, which relates to a flooding event, developed mainly in the transition zone of Cycle IV and Cycle V. The pinnacle represents the second depositional phase stratigraphically of Cycle V age. Volumetrically, it comprises the main buildup and the build-in structure of the buildup. It is compartmentalized vertically by two slightly tighter and muddy interbeds. These layers are thought to represent smaller flooding events [5].

3. Materials and Methods

3.1. Core and Log Data

Log data coverage includes exploration and production wells. Ten vertical wells have been interpreted as the main carbonate reservoir formations with full coverage. The core data are available in E11-2 and E11-3, as indicated in Table 1.

Table 1. Available data from the exploration and development wells in the E11 carbonate field (In X the available data).

Field	Well	Spud Year	GR	NGS	SP	CAL	RES	DEN	NEU	DTS	Shear Sonic	RFT/FMT	Core
E11	E11-1		X		X	X	X	X		X		X	
	E11-101		X	X	X	X	X	X	X	X			
	E11-102	1983	X	X	X	X	X	X	X	X		X	
	E11-105	1983	X	X	X	X	X	X	X			X	
	E11-107		X	X	X	X						X	
	E11-108	1983	X	X	X	X	X	X	X				
	E11-109	1983	X	X	X	X	X	X	X				
	E11-112	1983	X	X	X	X	X	X	X			X	
	E11-2	1983	X		X	X	X	X	X			X	X
	E11-3	1983	X		X	X	X	X	X			X	X

3.2. Multiscale Methodology

The workflow used for this study includes the following steps Figure 4:

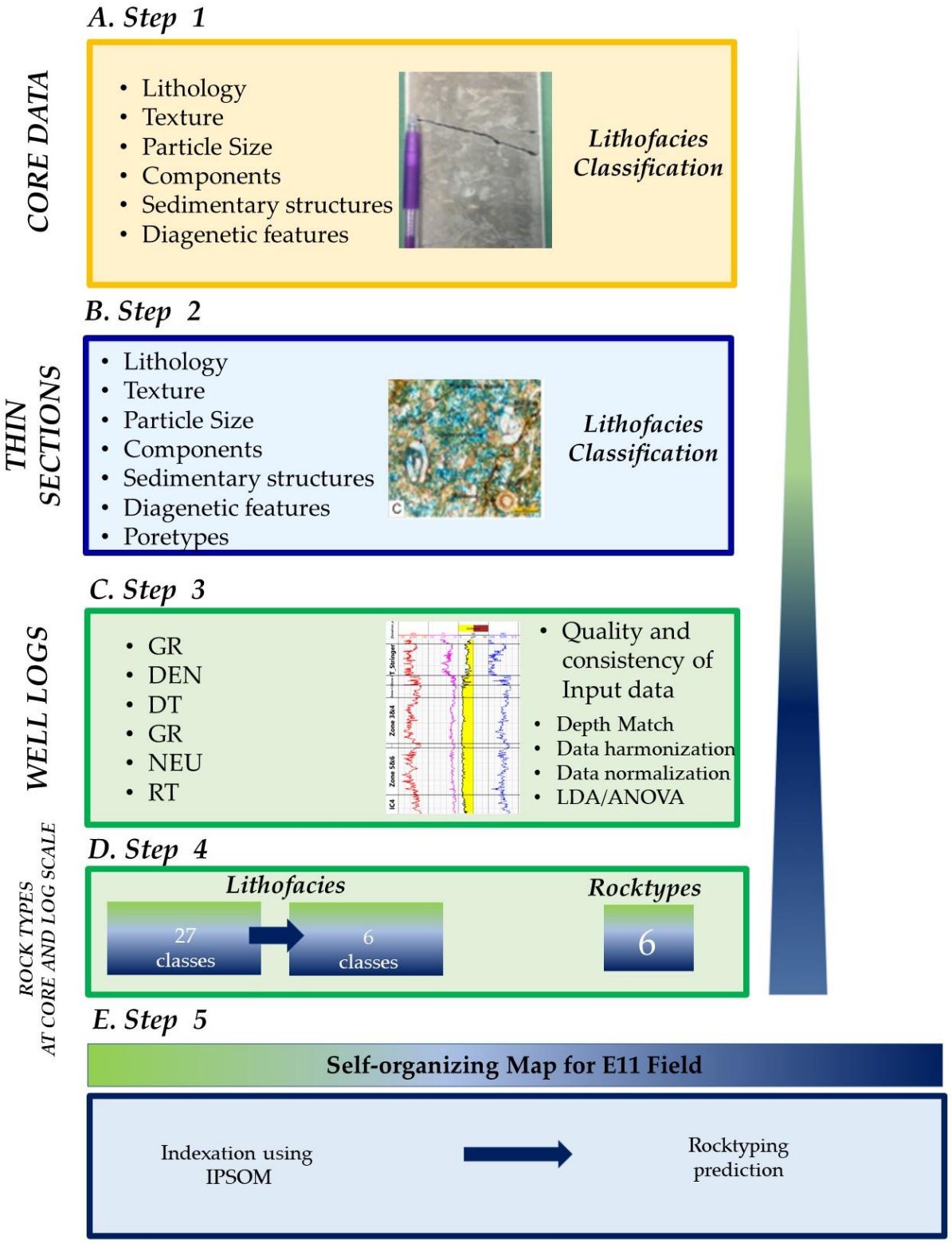


Figure 4. The workflow used for this study. (**A**) Step 1: Core data description, (**B**) Step 2: Thin section description, (**C**) Step 3: Well log interpretation, (**D**) Step 4: Lithofacies and Rocktypes interpretation, and (**E**) Step 5: IPSOM probabilized self-organizing maps for facies prediction SOM.

(a) Step 1: Core Data Description

A detailed sedimentological description was made for two cored wells of the Miocene E11 field at the Petronas Geo Sample Centre in 2017: E11-2 with a length of 339.55 m and EX-3 with 288.65 m. A detailed description of several attributes was made, as detailed in Table 2. Based on the description, 27 lithofacies were identified, as shown in Table 3, and they were upscaled to 6 groups of lithofacies Table 4.

Table 2. Attributes for sedimentological logging.

Lithology	argillaceous and non-argillaceous limestone, dolo-limestone, dolostone, and shale
Texture	mudstone, wackestones, packstone, grainstone, floatstone, rudstone, framestone, and bindstone
Particle size	clay, silt; fine, medium, and coarse arenite and rudite
Components	massive, branching, and platy corals, coralline red algae, benthic foraminifera, bivalves, brachiopods, bryozoans, gastropods, oncoids, skeletal debris, intra-clasts, and echinoids (0: absent, 1: rare, 2: common, 3: abundant).
Sedimentary structures	bioturbation (0: absent, 1: rare, 2: common, 3: abundant), micro-karst, karst features, rootlets
Diagenetic features	stylolite frequency per foot: 1 (1), 2 (2 to 3), 3 (4 to 10), 4 (11–30), 5 (>30); horsetails, solution seams (0: absent, 1: rare, 2: common, 3: abundant); mechanical compaction, dissolution/leaching, cementation, and recrystallization

(b) Step 2: Thin Section Description

For the thin section analysis, 100 thin sections were described from plug samples from the E11-2 core and 68 from the E11-3 core. They were analyzed using a transmission light microscope Olympus BX43F with an attached Olympus DP72 camera to determine the mineralogical composition, sedimentary and diagenetic features, and component composition.

(c) Step 3: Well Log Harmonization, Normalization, and Interpretation

The log data coverage comprises 10 wells, exploration/appraisal and development wells. A summary of the available logs is displayed in Table 1. The exploration wells are mainly vertical and provide full coverage, as observed during the core description. The development wells are named after 101; most of them have been directionally drilled as deviated in target zones of the reservoir.

The wireline log data are considered reliable. The first stage is to harmonize the data. This stage implied renaming several curves to recognize the curve types before they could be interpreted. The second stage is to verify the consistency of the data as well as the depth match normalization of DEN, GR, NEU, and DT logs. The normalization initially identifies and removes systematic errors from well log data so that reliable results can be obtained. The normalization includes well-to-well comparisons using histograms, cross plots, depth plots, and statistical measurements to reduce the disparity between vintage petrophysics tools. Finally, an analysis of variance is made to verify that petrophysics logs can segregate between the rock types and to reduce the data redundancy.

(d) Step 4: Lithofacies and Rock Typing Analysis

An initial rock type scheme of 27 lithofacies is presented Table 3. However, from a petrophysical and rock property perspective, the rocks are relatively simple, and the scheme can be simplified significantly for petrophysical evaluation purposes. Reducing the number of groups increased the predictability in IPSOM Table 4.

The rock typing combined the information from cores, and contrasted against well log measurements within a stratigraphy framework for every interval. A scheme of 6 rock

type groups Table 5 is sufficient to capture the most important petrophysical and geological controls on rock property distribution.

Table 3. List of 27 lithofacies types used to describe the E11 field.

1	Shale	LTF1
2	Mudstone to wackestone (skeletal)	LTF2
3	Mudstone to wackestone (red algae)	LTF3
4	Wackestone (skeletal)	LTF4
5	Wackestone (coral)	LTF5
6	Wackestone (red algae)	LTF6
7	Wackestone (benthic foraminifera)	LTF7
8	Wackestone to packstone (skeletal)	LTF8
9	Wackestone to packstone (coral)	LTF9
10	Wackestone to packstone (red algae)	LTF10
11	Wackestone to packstone (benthic foraminifera)	LTF11
12	Packstone (skeletal)	LTF12
13	Packstone (coral)	LTF13
14	Packstone (red algae)	LTF14
15	Packstone (benthic foraminifera)	LTF15
16	Packstone to grainstone (skeletal)	LTF16
17	Packstone to grainstone (coral)	LTF17
18	Packstone to grainstone (benthic foraminifera)	LTF18
19	Grainstone (benthic foraminifera)	LTF19
20	Floatstone (coral)	LTF20
21	Floatstone to rudstone (coral)	LTF21
22	Floatstone to rudstone (red algae)	LTF22
23	Rudstone (coral)	LTF23
24	Rudstone (red algae)	LTF24
25	Rudstone (benthic foraminifera/skeletal)	LTF25
26	Rudstone to framestone (coral)	LTF26
27	Framestone (coral)	LTF27

Table 4. List of 6 lithofacies types used for IPSOM map construction.

1	Shale	LTF1
2	mudstone/wackestone (skeletal debris)	LTF2
3	wackestone to packstone (red algae/foraminifera)	LTF3
4	packstone (coral/red algae/foraminifera)	LTF4
5	packstone to grainstone/grainstone (coral/red algae/foraminifera)	LTF5
6	floatstone (coral/red algae)	LTF6

Table 5. List of 6 Lithofacies types used for IPSOM map construction.

1	Dense argillaceous shale	R1
2	Cemented argillaceous limestone	R2
3	Mouldic limestone	R3
4	Chalkified limestones	R4
5	Sucrosic dolomites	R5
6	Mouldic sucrosic dolomites	R6

(e) Step 5: IPSOM: Probabilized Self-Organizing Maps for Facies Prediction SOM

The IPSOM is a 2D indexed and probabilized self-organizing map the Kohonen algorithm tool in Techlog software by Schlumberger, designed for the geological interpretation of well data and facies prediction. It is a popular clustering algorithm that provides a two-dimensional representation of a multidimensional dataset.

The tool is based on the classification of the training node, and the Euclidian distance is used to propagate the classification to the other nodes. This converts multi-dimensional well log data into a 1D and 2D discrete map [19]. The sub-steps are:

(a) Verify the quality and consistency of the well-input data (wireline and facies logs).
(b) Activate SOM to sort and organize the data into bins within which the multivariate data "patterns" are similar to each other.
(c) Assign a class name to each bin indexation.
(d) Refine the representation using the core log calibration data to improve the prediction.
(e) Finally, a trained IPSOM model is produced to propagate the rock type logs in the wells without available core data.

4. Results

4.1. Lithofacies/Rock Types of Analysis

The lithology in E11 was affected by diagenesis, as observed during the core description Figure 3. Three main basic lithologies are present in the E11 field: limestone 53%, dolomite 11%, and claystone 3%. The correlation among wells can only be achieved based on gamma-ray, neutron-, and density logs. The correlation was made in terms of flooding intervals. This led to the division of the carbonate into four porous zones (SS1, SS2, SS3, and SS4 separated by four tight layers FS1, FS2, FS3, and FS4, which are interpreted as major flooding intervals Figure 5. The E11 field can be subdivided into six basic rock types.

- **Dense argillaceous shale RT1**, from fair to poor reservoir rocks porosity of 10–25%, permeability 1–100 Md.
- **Tight argillaceous limestone RT2** is considered the poorest reservoir rock porosity 2–8% and permeability of 1–5 Md. From the core observation, these intervals are considered tight thin intervals, formed by the abundant occurrence of massive crystalline corals or intermittent emergence horizons (Figure 6B).
- **Mouldic limestone RT3**, a rock type that forms thick intervals of good reservoir quality. Porosities are 20–40% and permeabilities 10–400 mD (Figure 6C).
- **Chalkified limestones RT4** are widespread and constitute reservoirs with porosities ranging between 10 and 25% and permeabilities between 5 and 50 Md. Their porosity originated from fine interparticle microsolution chalkification (Figure 6D).
- **Sucrosic dolomites RT5**, from equally good reservoir rocks as mouldic limestones but, on a regional scale, they are less abundant than the latter. The sucrosic dolomites originated from mud-supported carbonates and have porosities of 15–30% and permeabilities of 10–500 mD (Figure 6E).
- **Mouldic sucrosic dolomites RT6** exhibit fossil mould in addition to their intercrystalline porosity. They form excellent reservoir rocks but have a limited distribution not exceeding 10% of the total rock volume. Porosities are 25–40% and permeabilities 100–3000 mD (Figure 6F).

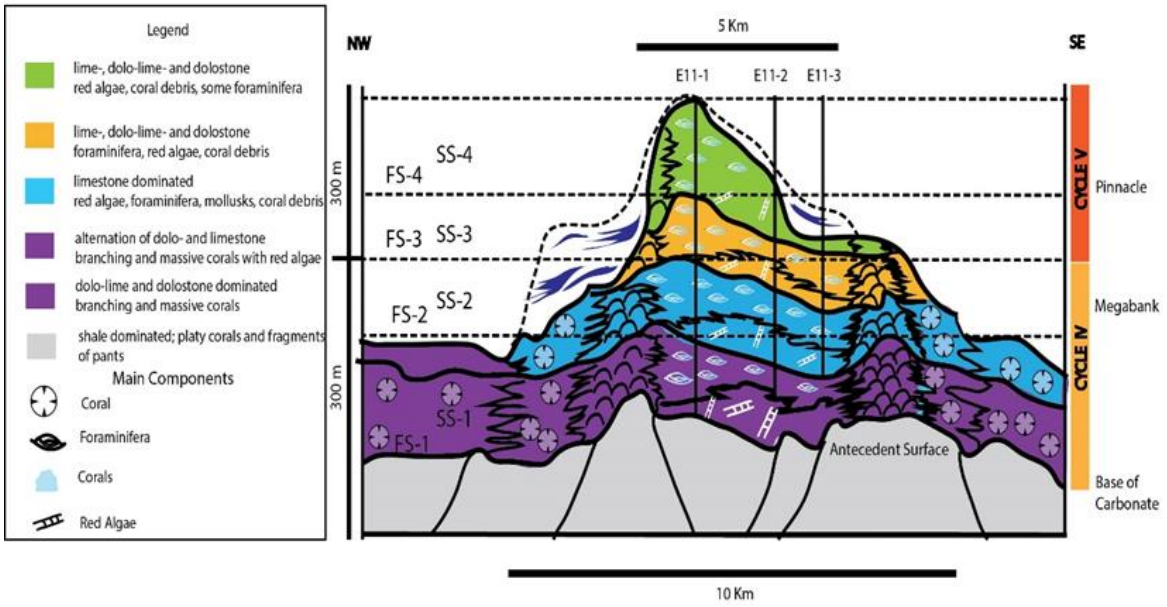


Figure 5. The lithological distribution model of the E11 platform and stratigraphic intervals.

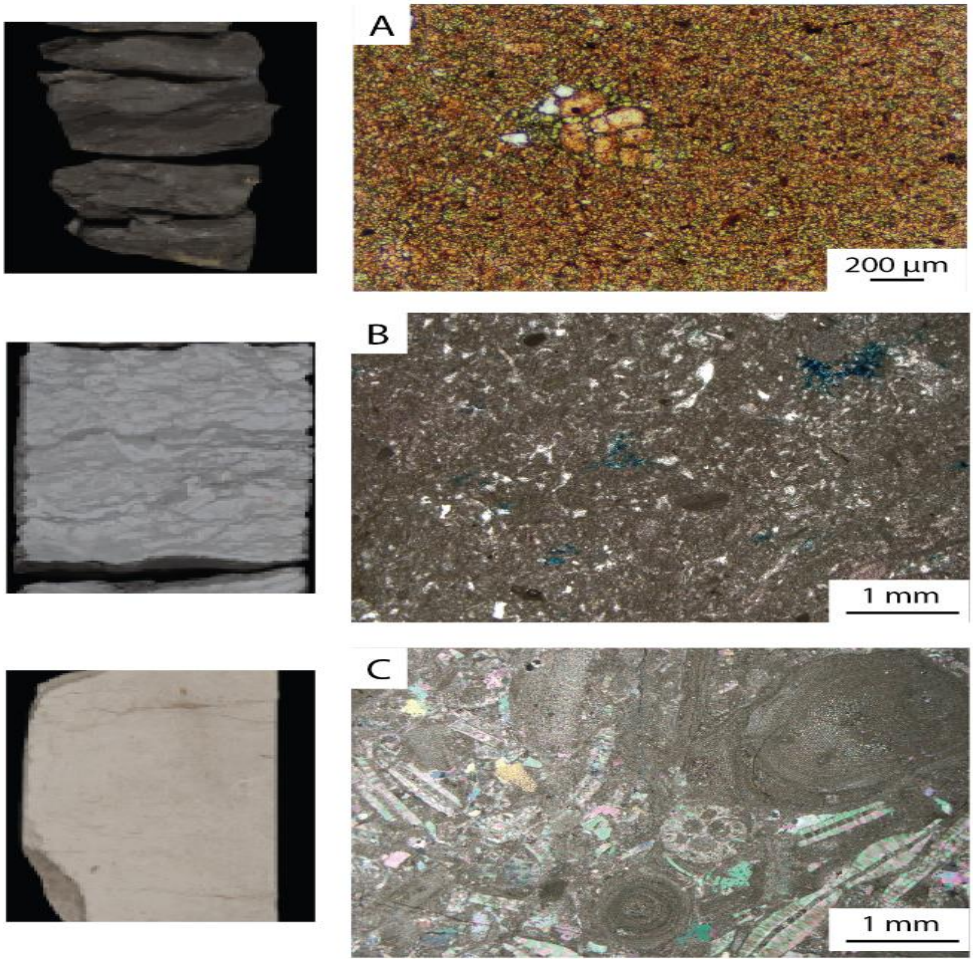


Figure 6. *Cont.*

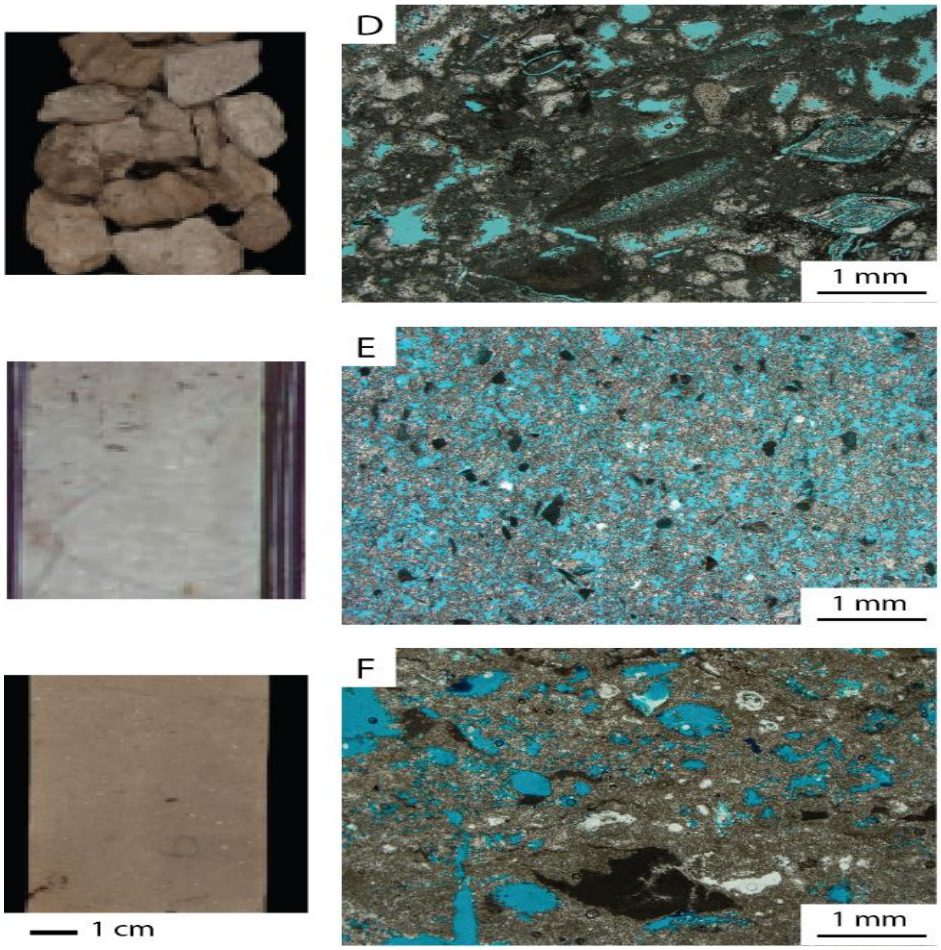


Figure 6. Core and thin sections of rock types: (**A**) dense argillaceous shale (RT1), (**B**) cemented argillaceous limestone (RT2), (**C**) mouldic limestone (RT3). (**D**) chalkified limestone (RT4), (**E**) sucrosic dolomite RT5, and (**F**) mouldic sucrosic dolomite RT6.

(a) Sequence SS1 Cycle IV

Most of this sequence is deposited over a carbonate megabank and consists of chalkified fine-grained limestones (mudstones, wackestones, and packstones) alternating with smaller amounts of sucrosic dolomites and tighter over-dolomites. We observed a trend with decreasing gamma-ray and density can be observed from bottom to top. The succession is mainly dominated by argillaceous limestone at the bottom FS1 and tight dolomite. Towards the top of the interval, the same can be assumed for E11-3, and thus a lateral extent of these layers of at least 2.6 Km.

This sequence tends to have a laterally more persistent reservoir quality, with the average gross porosities ranging between 17% in E11-2 and E11-3 and 21% in E11-1. The rest of the porosity consists of argillaceous limestones.

At the top of this sequence, an FS2 interval is present with foraminiferal limestone packstones and partially argillaceous lime wackestones with cemented coral fragments. The compaction features, such as horsetails and stylolites, are common. The unit is present throughout the buildup area, with a uniform thickness in the region of 45–52 m. Although the average porosities in the wells range between 7 (E113) and 14%, the unit contains tighter streaks that render it overall a poor reservoir rock. The tighter part (FS2) of the unit is assumed to act as a permeability barrier to production due to the lower permeability values (Figure 7).

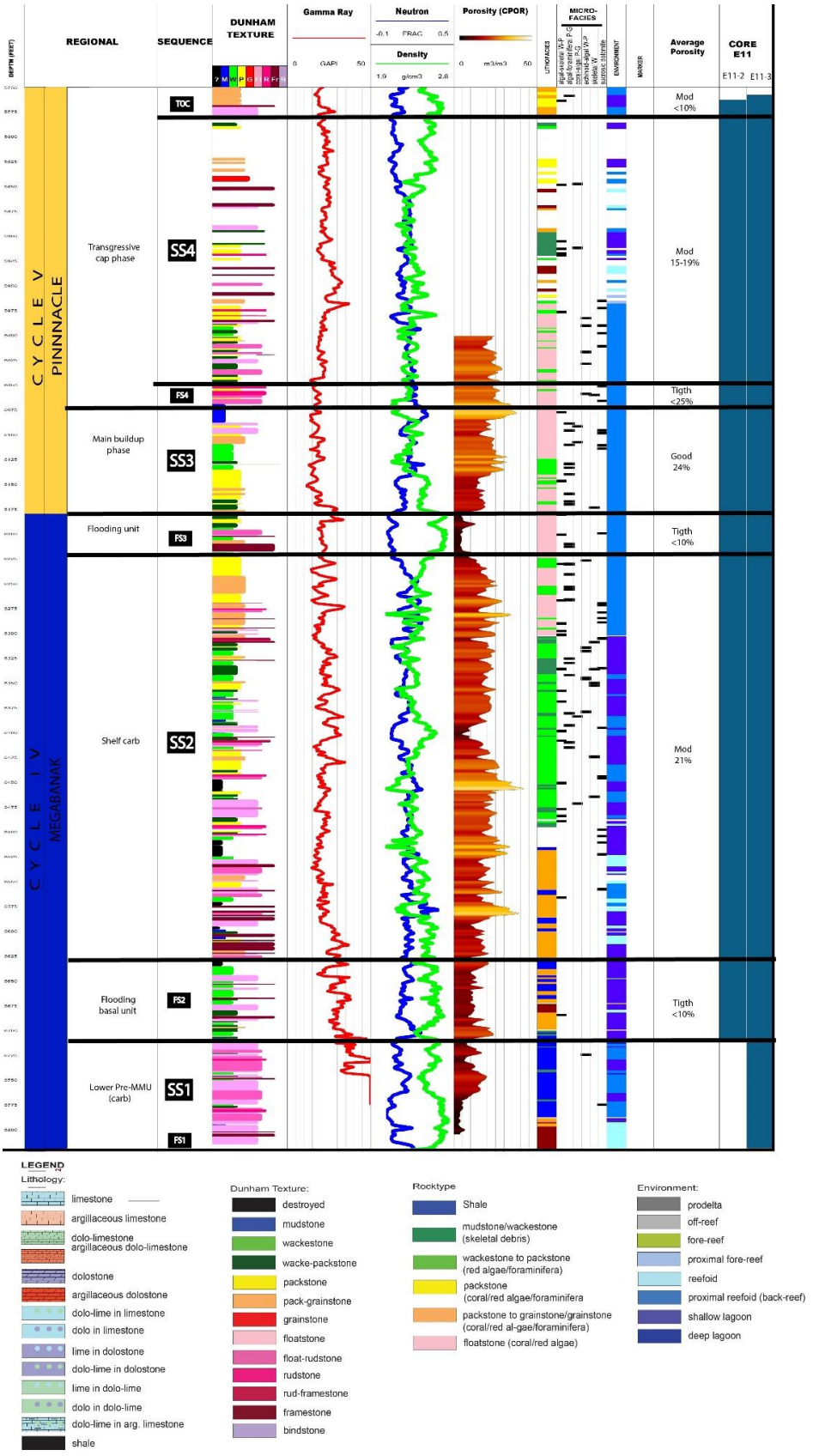


Figure 7. Composite well logs of E11-2. The logs are digitized and visualized using the software Well CAD. Description of the cores includes grain size, lithology, Dunham texture, gamma-ray, neutron, and density, porosity from core plugs, interpreted lithofacies, microfacies, and environment.

(b) Sequence SS2 Cycle IV

In this interval, the gamma-ray shows thin peaks, which again seem to coincide with the few occurrences of dolo-limestones in E11-2. The lower part with high-gamma-ray values consists of coralline red algae and minor benthic foraminifera pack-to-grainstone. There are predominantly mouldic/sucrosic (calcitic) dolomites (packstones to grainstones), with some sucrosic/mouldic dolomites (mudstones to wackestone).

The reservoir quality is related to the degree of dolomitization and is generally good, with the average gross porosity ranging from 21% in E11-2 to 21% in E11-1. The reservoir quality tends to be laterally persistent. An overall increase in gamma-ray and density is observed towards the top of the interval, where argillaceous limestones are present (FS3). This increase is also present in E11-3 but can only be explained in the upper part by the presence of an argillaceous interval.

(c) Sequence SS3 Cycle IV

The sequence consists of foraminiferal limestone packstones and partially argillaceous lime wackestones with cemented coral fragments. The unit is present throughout the buildup area, with a uniform thickness in the region of 10–15 m.

The density and gamma-ray values continue to decrease and rise again towards the upper boundary, which is defined at the base of the argillaceous limestone FS4. It is observed in the gamma-ray log that thin peaks are present in the upper half, which coincide with dolo-limestone and dolostone layers, which seem to correlate between several wells.

(d) Sequence SS4 Cycle V

An alternation of tight and chalkified or mouldic lime packstones is observed with some reefoid to protect influences in the crestal area E11-1. The average porosity ranges from 8% in E11-2 to 19% in E11-1.

We observe in both wells constant gamma-ray values with a slight increase at the top, especially in E11-2. A connection between the occurrence of dolostone and an increase in gamma-ray seems to be present in E11-2. Meanwhile, in E11-2, wacke- and packstone with mainly coralline red algae and minor benthic foraminifera and skeletal debris dominate, and E11-3 is dominated by float- and rudstones with coral debris.

4.2. Self-Organizing Maps

(a) Neural Analysis

We performed clustering of the inputs to obtain a downsampled but representative set of "nodes". The SOM structure comprises a single-layer linear 2D grid of neurons, instead of a series of layers. The SOM was used to cluster the well data into six rock type classes, as shown in Figure 8. The clustering was carried out using a two-level approach, where the data set was first clustered using the SOM, and then the SOM was finally clustered. These results are only valid if the clusters using the SOM are similar to those of the original data.

(b) Model Propagation

The model can be refined using various iterations and parameter input/output to arrive at reasonable clusters. The last step is to apply the refined the IPSOM model to the well log dataset over the entire interval to create "rock type" classification curves Figure 9. These can be appropriately named and color-coded. The zone-by-zone classification results on a well are shown in the graphic below.

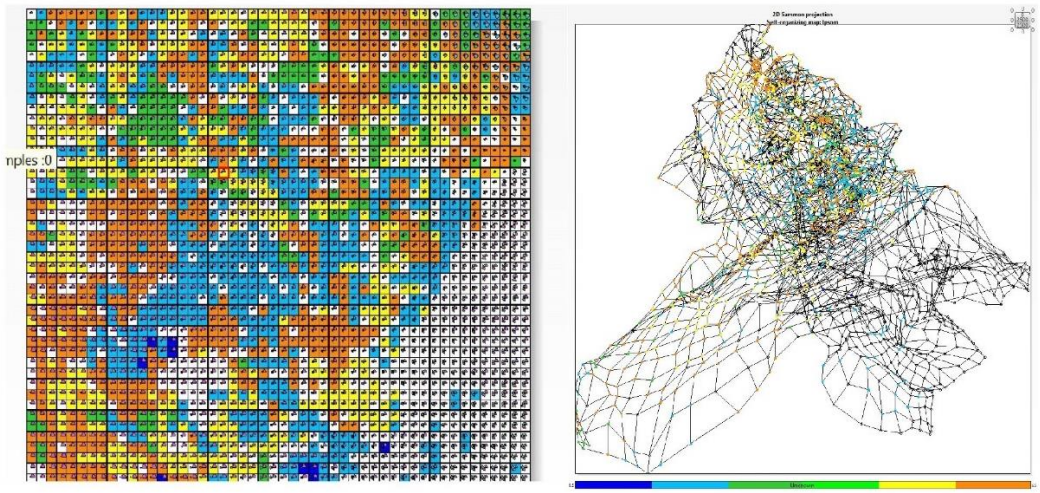
The predictable variability of rock type gives confidence that the technique can be usefully applied to a larger dataset of eight remaining wells without core data Figures 10 and 11.

(c) Correlation

The relationship between the predicted "rock types" and the rock types from core log scale is evidenced in the correspondence analysis.

The correlation between core data and log for E11-2 gave a Cramer's index of 80%, a good success rate of predicting the correct core-based rock type from log data with the

model. The depth plots of the predicted rock type show close correspondence to the core-based rock types in terms of stratigraphic organization, proportions, and juxtaposition. This result is sufficiently good to merit the application of the model to the E11 field Table 6.



(**A**) (**B**)

Figure 8. (**A**) IPSOM classification. (**B**) 2D Sammon projection.

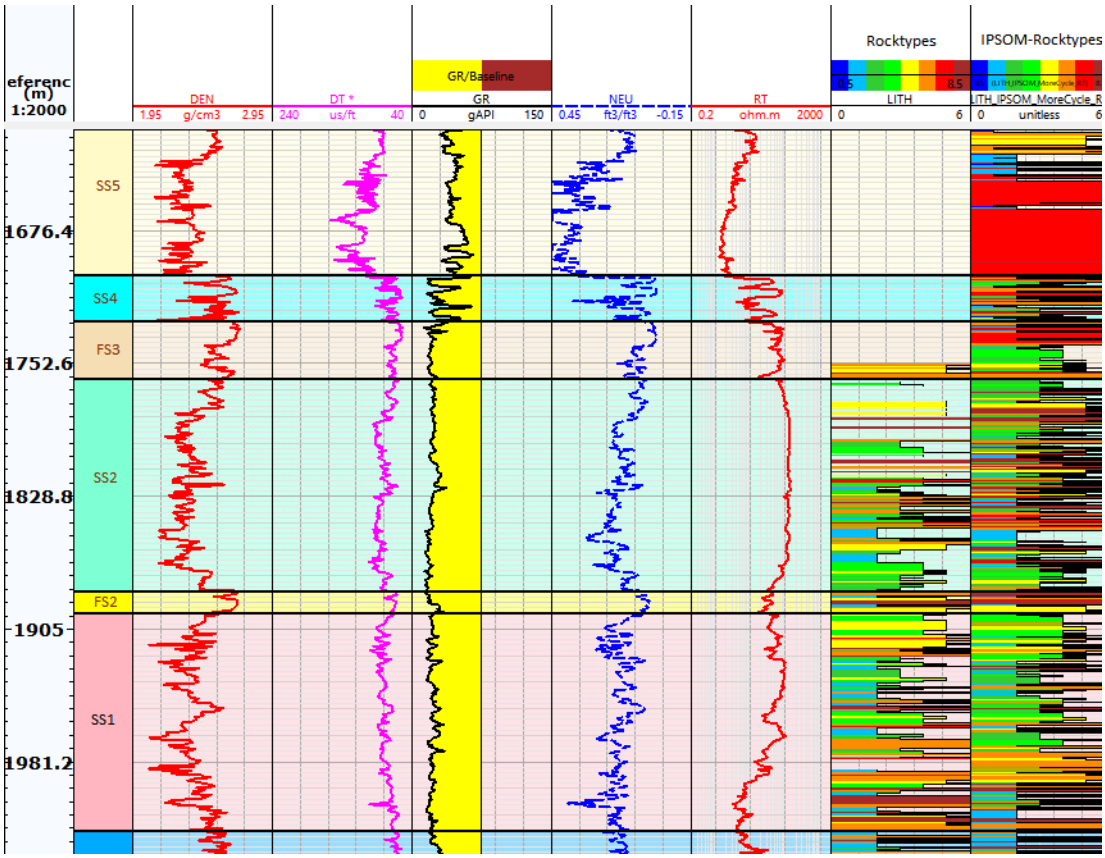


Figure 9. The above graphic shows a log facies of the E11-2 plot. The 6 rock types were computed using IPSOM probabilized self-organizing method. The track on the right (Column 8) is color-coded for facies 1 to 6. The input logs are bulk density, compressional slowness, gamma-ray, neutron porosity, and resistivity.

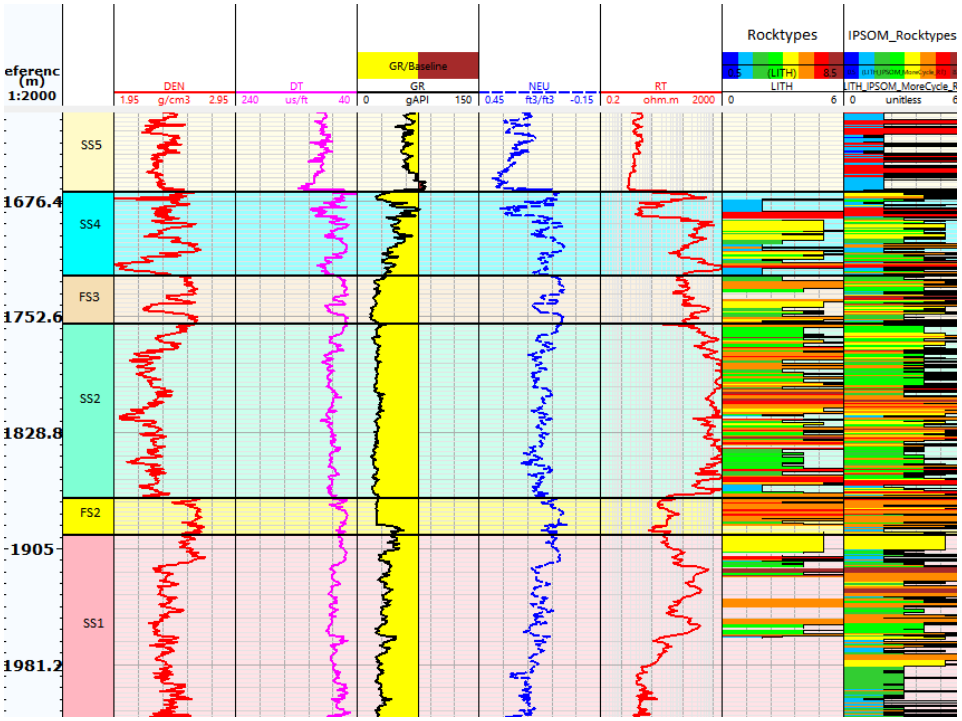


Figure 10. The above graphic shows in Column 8 the predicted rock types of E11-3.

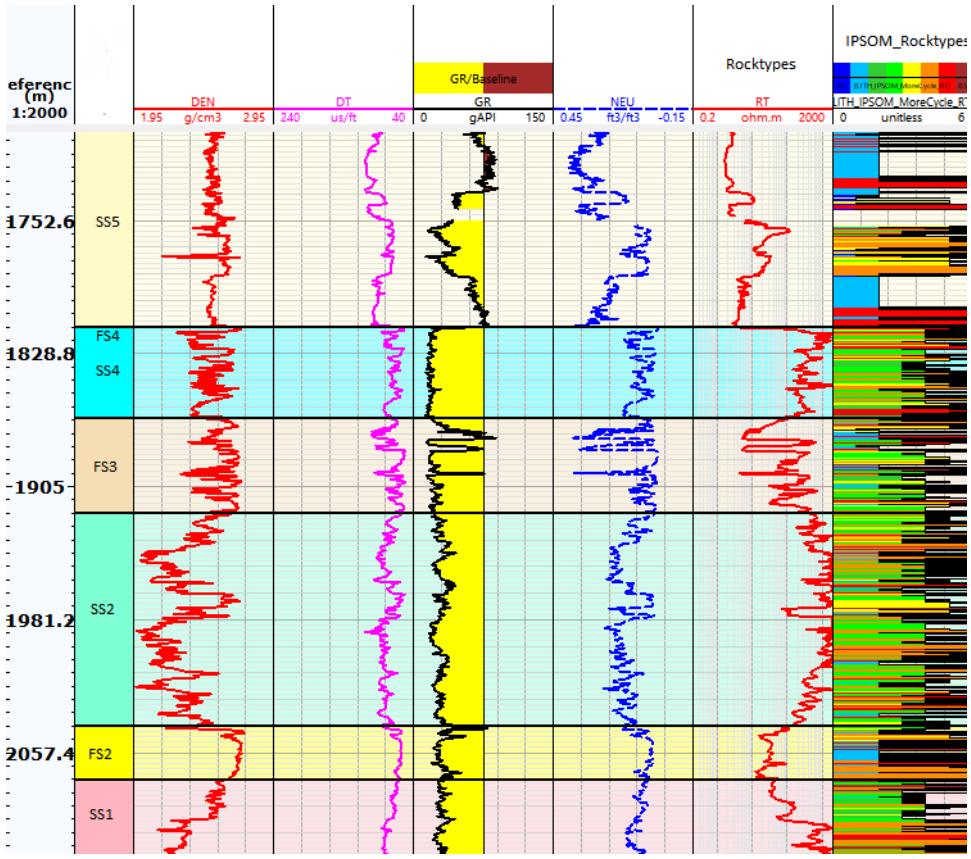


Figure 11. The above graphic shows in Column 8 the predicted rock types of E11-101.

Table 6. The relationship between the predicted rock types (x) and the reference rock type from the core (y).

	RT1	RT2	RT3	RT5	RT6	Total
RT1	17				6	23
RT2		474	5	21	26	526
RT3		11	177	15	7	210
RT5		24	20	497	29	570
RT6	3	62	13	35	699	812
Total	20	571	215	568	767	2141

5. Discussion

The spatial distribution of porous and tight carbonates in the buildup is still, to a large extent, controlled by the primary environment of deposition but preferentially transformed by dolomitization and freshwater stabilization [9].

The present study shows that the porosities in E11 are mainly of the sucrosic intercrystalline, mouldic, and chalky types. Overall, mud-rich packstones, wackestones, and clay-lean mudstone at SS1, SS2, SS4, and SS5 seem not affected by intense early cementation; however, they were dolomitized and selectively leached, as observed in the core (RT4, RT5, RT6). The dolomite was found in appreciable quantities in the two cored wells, with improved reservoir quality generally associated with it. The lower part of Cycle IV SS1, however, is partially over-dolomitized, with a consequent deterioration in reservoir quality associated with this process. Due to the frequent alternation between the reef and bank settings during buildup growth, especially in the upper sections of many buildups SS2, SS3, and SS4, the change in reservoir quality in the vertical sense is more pronounced than in the lateral sense.

The core plugs' porosities range between 5 and 45%. The whole core vertical permeabilities obtained from the tightest intervals, including the porosity of FS4, are less than 0.01 mD. As shown by the well data, the average reservoir quality tends to deteriorate from the crestal area toward the flanks, but not to the same degree for the different porosity zones.

It is observed that the predicted rock types of logs Table 5 can be correlated among the different wells. The correlation helped us to understand the lateral and vertical distribution among the field.

A very important finding is that the rock type correlation proved the presence of flooding layers. These layers can be related to flooding or exposure intervals. Several flooding tight layers FS1, FS2, FS3, FS4 can act as baffles to vertical flow during production, depending on the relative amount of cementation vs. karstification [9]. On seismic argillaceous wackestones, intervals often correlate to backstepping geometries. Similar geometry patterns were observed in the Jintan platform [20]. This evidence suggests that the argillaceous, low-porosity layers were caused by flooding events when the relative sea level rose faster than the growth, where the platform shrank in size [9]. These intervals are mainly dominated by RT1 and RT2 rock types. Mud-lean packstones, grainstones, and clay-rich mudstones were essentially unaffected by dolomitization and corrosion (leaching) because they were tight due to either early cementation or their originally low permeability. This resulted in poor reservoir quality RT2and may have a strong influence on the dynamics of the field. Characterizing this may help to reduce uncertainty, which is very important, especially when petrophysical rock types are the basis of computing the initial fluid saturations at each grid node and assigning dynamic properties such as relative permeability curves in reservoir simulations [21].

6. Conclusions

The core well data calibration and the IPSOM probabilized self-organizing maps are powerful tools for electro log-based facies analysis as they provide an organized workflow for selecting, processing, and analyzing data consistently and with promptness. Looking

at the cross plots and histograms generated by IPSOM, this workflow proved to be a useful method to better visualize data, remove data noise, and correlate wells for a better understanding of the rock types of distribution in the E11 field.

Based on the evidence from the core, lithofacies, and the rock types, the E11 field is the result of a complex late diagenetic sequence of dolomitization, which has proven to be the main factor determining the rock typing and, later, the propagation.

The current analysis also provides a strong link between log-derived rock types and core-based definitions of a complex late diagenetic sequence of dolomitization. This should assist in the understanding of the 3D distribution of rock types over the field. The distinction between tight layers and porous zones would aid in saturation prediction and future geological modeling.

Author Contributions: Conceptualization, G.J.S., M.P.; methodology, G.J.S., W.B.H.; software, G.J.S., W.B.H.; validation, G.J.S., W.B.H.; formal analysis G.J.S., S.B.B.; resources, A.H.A.L.; writing—original draft preparation, G.J.S.; writing—review and editing, G.J.S., A.H.A.L., M.P.; visualization, G.J.S., W.B.H.; supervision, A.H.A.L.; project administration, A.H.A.L.; funding acquisition, A.H.A.L. All authors have read and agreed to the published version of the manuscript.

Funding: This research was funded by Murata grant: 015ME0-242 and PRG grant: 015PBC-021.

Acknowledgments: The authors acknowledge the full support of the Centre for Subsurface Imaging in completing this study. We also acknowledge PETRONAS's Malaysian Petroleum Management (MPM) for allowing the publication of this work, and the following software companies for providing academic licenses: Schlumberger for providing TECHLOG, PETREL, Eliis for Paleo Scan TM software, and Advance Logic Technology (ALT) for providing the Well CAD software used to conduct this research.

Conflicts of Interest: The authors declare no conflict of interest.

References

1. Epting, M. The Miocene carbonate buildups of central Luconia, offshore Sarawak. In *Atlas of Seismic Stratigraphy*; Bally, A.W., Ed.; AAPG: Tulsa, OK, USA, 1989; pp. 168–173.
2. Wilson, M.E. Cenozoic carbonates in Southeast Asia: Implications for equatorial carbonate development. *Sediment. Geol.* **2002**, *147*, 295–428. [CrossRef]
3. Epting, M.; Berhad, L.S.S. Sedimentology of Miocene Carbonate Buildups, Central Luconia, Offshore Sarawak. *Bull. Geol. Soc. Malays.* **1980**, *12*, 17–30. [CrossRef]
4. Bracco Gartner, G.L. High-Resolution Impedance Model of Outcrops and Their Application in Seismic Interpretation. Ph.D. Thesis, Vrije Universiteit, Amsterdam, The Netherlands, 2000; pp. 105–123.
5. Zampetti, V.; Schlager, W.; van Konijnenburg, J.-H.; Everts, A.-J. Architecture and growth history of a Miocene carbonate platform from 3D seismic reflection data; Luconia province, offshore Sarawak, Malaysia. *Mar. Pet. Geol.* **2004**, *21*, 517–534. [CrossRef]
6. Jamaludin, S.F.; Pubellier, M.; Menier, D. Relationship between syn-depositional faulting and carbonate growth in Central Luconia Province, Malaysia. *Bull. Geol. Soc. Malays.* **2014**, *60*, 77–83. [CrossRef]
7. Ali, S.H.; Poppelreiter, M.C.; Shah, M.M.; Saw, B.B.; Schlaich, M. Diagenetic understandings based on quantitative data, Miocene carbonate buildup, Offshore Sarawak Malaysia. *Pet. Coal* **2018**, *60*, 1275–1282.
8. Rankey, E.C.; Schlaich, M.; Mokhtar, S.; Ghon, G.; Ali, S.H.; Poppelreiter, M. Seismic architecture of a Miocene isolated carbonate platform and associated off-platform strata (Central Luconia Province, offshore Malaysia). *Mar. Pet. Geol.* **2019**, *102*, 477–495. [CrossRef]
9. Warrlich, G.; Adams, E.; Ryba, A.; Tam, T.; Ting, K.; Tang, H. What matters for flow and recovery in carbonate gas reservoirs: Insights from the mature Central Luconia Province, offshore Sarawak, Malaysia. *AAPG Bull.* **2019**, *103*, 691–721. [CrossRef]
10. Jiménez Soto, G.; Latiff, H.A.; Poppelreiter, M.C.; Rahmatsyah, K.; Rahman, S.; Bing, S.B.; Habel, W.B. Application of Spectral Decomposition as a Tool for Carbonate Geobodies Extraction. In Proceedings of the 82nd EAGE Annual Conference & Exhibition, Amsterdam, The Netherlands, 18–21 October 2021; Volume 2021, pp. 1–5.
11. Vahrenkamp, V.C. Miocene carbonates of Luconia Province, offshore Sarawak: Implication for regional geology and reservoir properties from strontium isotope stratigraphy. *Bull. Geol. Soc. Malaysia.* **1998**, *42*, 1–13. [CrossRef]
12. Skalinski, M.; Kenter, J.A.M. Carbonate petrophysical rock typing: Integrating geological attributes and petrophysical properties while linking with dynamic behaviour. *Geol. Soc. Lond. Spéc. Publ.* **2014**, *406*, 229–259. [CrossRef]
13. Jolley, S.J.; Fisher, Q.J.; Ainsworth, R.B. Reservoir compartmentalization: An introduction. *Geol. Soc. Lond. Spéc. Publ.* **2010**, *347*, 243–255. [CrossRef]

14. Ahr, W.M. *Geology of Carbonates: The Identification, Description, and Characterization of Hydrocarbon Reservoirs in Carbonate Rocks*; John Wiley & Sons: Hoboken, NJ, USA, 2008.
15. Ghon, G.; Grana, D.; Rankey, E.C.; Baechle, G.T.; Bleibinhaus, F.; Lang, X.; de Figueiredo, L.P.; Poppelreiter, M.C. Bayesian facies inversion on a partially dolomitized isolated carbonate platform: A case study from Central Luconia Province, Malaysia. *Geophysics* **2021**, *86*, B97–B108. [CrossRef]
16. Wong, L.J.; Mohamad, A.H.; bt Ishak, N.A.; Shields, D.J.; Ali, F.H.B.; Amdan, A.B.; Panting, A.T.P. Rock Typing for a Carbonate Gas Field in Central Luconia Province—An Integrated Approach from Microscale to Macroscale. In Proceedings of the Third EAGE Integrated Reservoir Modelling Conference, Kuala Lumpur, Malaysia, 5–7 December 2016; Volume 2016, pp. 1–4.
17. Koša, E. Sea-level changes, shoreline journeys, and the seismic stratigraphy of Central Luconia, Miocene-present, offshore Sarawak, NW Borneo. *Mar. Pet. Geol.* **2015**, *59*, 35–55. [CrossRef]
18. Yusliandi, A.; Sautter, B.; Poppelreiter, M.C. The Various Controls on The Platform Architecture of Carbonate Buildups in the Central Luconia Province, Offshore Sarawak. *Pet. Coal* **2019**, *61*, 1425–1437.
19. Dixit, N.; McColgan, P.; Kusler, K. Machine Learning-Based Probabilistic Lithofacies Prediction from Conventional Well Logs: A Case from the Umiat Oil Field of Alaska. *Energies* **2020**, *13*, 4862. [CrossRef]
20. Jiménez Soto, G.; Arshad Berg, M.; Poppelreiter, M.C.; Rahmatsyah, K. Multiple Point Statistics Carbonate Facies Modelling Workflow using Core Data and Spectral Decomposition Attributes: A Case Study from TX Field in Central Luconia Province, Malaysia. *Pet. Coal J.* **2020**, *62*, 1209–1224. [CrossRef]
21. Gunter, G.; Sahar, M.Y.; Viro, E.; Negahban, S.; Allen, D.F. Introducing a ten-step integrated petro-physical rock type verification process that combines deterministic methods, saturation height modeling, advanced. In Proceedings of the Abu Dhabi International Petroleum Exhibition & Conference, Abu Dhabi, United Arab Emirates, 12–15 November 2018.